ACS MEASUREMENT SCIENCE Au
AN OPEN ACCESS JOURNAL OF THE AMERICAN CHEMICAL SOCIETY

pubs.acs.org/measureau

Article

# In Situ Confocal Raman Microscopy of Redox Polymer Films on Bulk Electrode Supports

Jiahe Xu, Miharu Koh, Shelley D. Minteer, and Carol Korzeniewski*

Cite This: *ACS Meas. Sci. Au* 2023, 3, 127−133

Read Online

ACCESS | Metrics & More | Article Recommendations | Supporting Information

**ABSTRACT:** A spectroelectrochemical cell is described that enables confocal Raman microscopy studies of electrode-supported films. The confocal probe volume (~1 $\mu m^3$) was treated as a fixed-volume reservoir for the observation of potential-induced changes in chemical composition at microscopic locations within an ~20 $\mu$m thickness layer of a redox polymer cast onto a 3 mm diameter carbon disk electrode. Using a Raman system with high collection efficiency and wavelength reproducibility, spectral subtraction achieved excellent rejection of background interferences, opening opportunities for measuring within micrometer-scale thickness redox films on widely available, low-cost, and conventional carbon disk electrodes. The cell performance and spectral difference technique are demonstrated in experiments that detect transformations of redox-active molecules exchanged into electrode-supported ionomer membranes. The in situ measurements were sensitive to changes in the film oxidation state and swelling/deswelling of the polymer framework in response to the uptake and discharge of charge-compensating electrolyte ions. The studies lay a foundation for confocal Raman microscopy as a quantitative in situ probe of processes within electrode-immobilized redox polymers under development for a range of applications, including electrosynthesis, energy conversion, and chemical sensing.

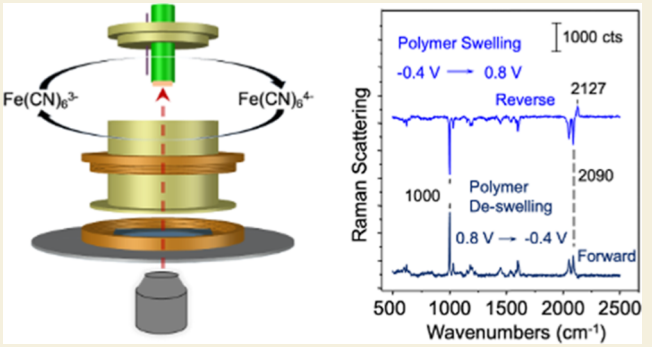


**KEYWORDS:** *Raman microscopy, redox polymer, polymer-modified electrode, confocal, thin film*

## INTRODUCTION

Electrode-supported redox polymer films have a long history[1,2] and continue to be important in the advancement of materials for applications that include energy conversion and storage, electrosynthesis, and chemical sensing (cf., refs 3−9). Strategies have focused on the development of polymers that mediate charge transport through a self-exchange-based electron conduction mechanism and remain active and stable during use.[3,4,10−12] Alongside the progress in synthetic approaches that improve current densities, polymer film durability, and, in the case of bioelectrocatalytic membranes—biocompatibility, have been improvements in methods for the study of processes that limit material performance.[1,2,5,10,11,13,14] Spectroscopic techniques capable of probing electrode-supported redox-active layers in real time under reaction conditions have been greatly sought-after.[5,11,15,16] Infrared and surface-enhanced Raman spectroscopy are well suited to in situ investigations of phases near monolayer coverages on electrodes. (cf., refs 17−23) In the study of thin film and multilayer materials, however, these vibrational spectroscopic techniques are not as easily adapted. Sensitivity is lost as surface-enhanced electromagnetic fields decay and spectral band distortions develop in response to optical dispersion effects.[15,24,25] As a step toward overcoming these limitations, we recently investigated confocal Raman microscopy for quantitative in situ measurements within electrode-supported redox polymer films.[26]

A confocal Raman microscope records spectra from microscopic spatial regions within a sample.[27−30] The objective brings the excitation beam to a tight, diffraction-limited spot (focal volume), and Raman scattered radiation is collected from the region through an aperture that restricts light from outside the focal volume from reaching the detector.[27−29] The dimensions of the aperture and excitation beam focus define the primary location probed within the sample. This so-called confocal probe volume region typically occupies a few femtoliters in measurements that employ high-numerical-aperture (NA) oil-immersion objectives.[28,29,31] In recent years, confocal Raman microscopy has emerged as a unique and powerful tool for conducting rapid, sensitive chemical assays based on detection within individual high surface area

Received: November 5, 2022
Revised: December 20, 2022
Accepted: December 21, 2022
Published: January 13, 2023

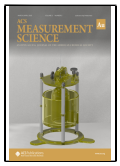





https://doi.org/10.1021/acsmeasuresciau.2c00064
*ACS Meas. Sci. Au* 2023, 3, 127−133

chromatographic particles (cf., refs 31−34). With the confocal probe volume positioned centrally within a particle, the analyte extracted into the pores can be easily quantified, label-free at subnanomole levels.[31−33] The latest work, centered on studies of DNA hybridization, has demonstrated spectral subtraction as effective for enhancing sensitivity.[33] Reflecting the high stability of the confocal probe volume, the difference measurements revealed exquisite details of base pairing and enabled detection at the level of a single nucleotide polymorphism.[33]

In our first adaptation of confocal Raman microscopy for in situ studies of processes at electrodes,[26] drawing from an earlier design,[35] the cell was fitted with an optically transparent, electronically conductive indium tin oxide (ITO)-coated coverslip that functioned as both the cell window and working electrode. After entering the cell through the coverslip, the confocal probe volume was positioned ∼3 μm from the ITO surface and served as a fixed-volume reservoir for the quantification of redox-active species within the diffusion layer.[26] The reported work advances the platform through modifications that enable the use of conventional disk electrodes, which are more widely available and have considerably better electronic conductivity than ITO-coated glass. Precision-machined, the cell operates with the working electrode surface held parallel to the cell window (Figure 1).

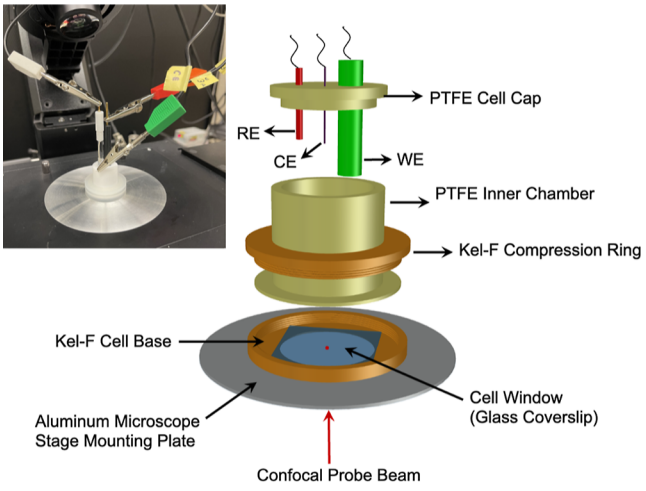


**Figure 1.** Sketch of the microscope stage mountable cell for confocal Raman microscopy studies of films supported on conventional disk electrodes. A photo of the cell on the microscope stage is shown on the inset. The working, counter, and reference electrodes are labeled WE, CE, and RE, respectively. See text for details.

As shown previously,[36] the ability to employ conventional disk electrodes greatly extends the application of confocal Raman microscopy for in situ studies of electrode processes and materials for energy and sensing applications. Herein, cell performance is demonstrated through studies of ionomer films containing exchanged redox ions supported on carbon electrodes. Using a Raman system with high collection efficiency and wavelength reproducibility, spectral subtraction[33,37] achieved excellent rejection of background carbon interferences and uncovered reversible swelling and deswelling of a polymer framework under the influence of an applied potential. The strategy opens opportunities for performing in situ measurements within micrometer-scale thickness redox-active films supported on conventional disk electrodes.[3−9,38]

## EXPERIMENTAL SECTION

### Reagents

Nafion perfluorinated resin (10 wt % in water, product number 527106), methyl viologen (MV) dichloride (98%), potassium hexacyanoferrate (III), and potassium chloride were obtained from Sigma-Aldrich (Saint Louis, MO, USA). Sustainion (XA-9, 5 wt % in ethanol) was obtained from Dioxide Materials (Boca Raton, FL, USA). All were of reagent grade or better purity and used as received. Aqueous solutions were prepared from 18 MΩ cm water dispensed from a Barnstead Nanopure UV water filtration system.

### Electrode-Supported Films

Just prior to film deposition, glassy carbon disk electrodes (3 mm diameter C disk (CHI-104 in 8.0 cm long sheath), CH Instruments, Austin, TX USA) were polished in a slurry of aluminum oxide powder (0.3 and 0.05 μm, Buehler, Bluff, IL) followed by copious rinsing in deionized water aided by brief sonication in an ultrasonic bath. Nafion films were deposited to ∼25 μm thickness by casting 15 μL from the stock dispersion. After allowing the film to reach dryness at 60 °C, the electrode was immersed in 1.0 mM $MV^{2+}$ for 10 min and subsequently rinsed in 0.1 M KCl before transfer to the spectroelectrochemical cell. Adherent Sustainion films (∼20 μm) were prepared similarly by casting from 15 μL of the stock reagent followed by drying under ambient temperature. The film-coated electrode was immersed in aqueous 40 mM $K_3Fe(CN)_6$ containing 0.1 M KCl for 10 min and subsequently rinsed in 0.1 M KCl before transfer to the spectroelectrochemical cell.

### Electrochemistry

A WaveNow (Pine Research, Durham, NC USA) potentiostat running AfterMath software was used to record cyclic voltammograms and control the electrode potential during Raman spectral measurements. A Pt wire shaped to form a ring at one end served as the counter electrode, and a KCl-saturated silver−silver chloride electrode was the reference. In experiments with $MV^{2+}$, the solution was degassed by bubbling with Ar and the cell was purged with Ar prior to measurements. All experiments were performed at ambient laboratory temperature (21.0 ± 0.5 °C).

### Confocal Raman Microscopy

The confocal Raman microscope was constructed based on earlier designs.[26,29] Details are given in the Supporting Information. Raman scattering was excited by a 660 nm single-mode diode-pumped solid-state laser [Gem 660 (0.75 ± 0.15 mm beam diameter), Laser Quantum, Fremont, CA, USA]. The laser beam was expanded (7×, Special Optics, Denville, NJ, USA) and directed toward the rear entrance port of an Olympus IX73 inverted microscope (Olympus, Waltham, MA, USA). The microscope objective [100×, 1.45 NA, Olympus (UPLXAPO, 130 μm working distance, 5.2 mm rear aperture)] brought the excitation radiation into the electrochemical cell through a film of immersion oil in contact with a glass microscope coverslip [no. 1.5 (0.17 mm thickness), BK-7 glass, 22 mm × 22 mm] that was mounted to the bottom of the cell (Figure 1). Backscattered Raman light was collected through the same microscope objective. After passage through a final long-pass filter (LP02-664RU-25, Semrock), the radiation was focused onto the entrance slit (50 μm) of a grating monochromator (Shamrock 500i, Andor, Belfast, UK). The diffraction grating, 300 lines/mm blazed at 760 nm, dispersed Raman scattered light from the slit image onto a charge-coupled device (CCD) camera (iDus DU416A, Andor). The resolution achieved was 1.66 $cm^{-1}$/pixel. The confocal aperture was defined using the entrance slit of the monochromator in the horizontal dimension and by binning three rows of pixels on the CCD camera (45 μm) in the vertical dimension.[28,39] Unless stated otherwise, the acquisition time for each spectrum was 60 s and the excitation laser power measured at the back of the microscope was 3 mW.

### Data Analysis

Spectral data were processed on desktop computers using custom scripts executed in MATLAB (version R2022a; MathWorks, Natick,


https://doi.org/10.1021/acsmeasuresciau.2c00064
ACS Meas. Sci. Au 2023, 3, 127−133

MA, USA). After subtraction of a dark current offset, Raman spectra were corrected for instrument response by ratioing to a recorded spectrum of emission from a standard reference halogen source lamp (SL1-CAL, StellarNet, Tampa, FL, USA).[40−42] Spectral baselines were corrected using a rolling-circle[43] high-pass filter. Further analysis and subtraction manipulations were performed using Microsoft Excel (Redmond, WA, USA) and OriginPro (Version 8.0, OriginLab Corp., Northampton, MA, USA).

## RESULTS AND DISCUSSION

The cell constructed for in situ confocal Raman microscopy studies of electrode-supported films was designed for the stage of an inverted microscope (Figure 1). A glass microscope coverslip serves as the optical window and forms the bottom of the electrolyte-filled reservoir. The coverslip is positioned within a chemically inert, electronically insulating base machined from the fluoropolymer Kel-F. A circular opening in the base allows light to pass to the window. The base is pressed into a microscope stage plate constructed from aluminum. A polytetrafluoroethylene (PTFE) cylinder fabricated with a flange at one end forms a chamber for the electrolyte solution. The cell is assembled by positioning the cylinder in the cell base with the flange against the coverslip. A Kel-F compression ring sandwiches the coverslip between the flange and Kel-F cell base to form a water-tight seal.

The electrodes are admitted to the cell through drilled holes in the PTFE cap. The cap was precision-machined to fit the open end of the PTFE cylinder and secure the electrodes snuggly with the disk working electrode surface oriented parallel to the plane of the glass coverslip. The working electrode is adjustable vertically. The objective working distance is sufficient to enable free transport into the electrode-window gap, contrasting the thin-layer configuration (~5 $\mu$m) that can limit mass transport and accuracy in potential control in in situ reflectance infrared measurements.[16,44] There is also flexibility to add ports to the cap for sample introduction and removal and to facilitate measurements under an inert atmosphere.

Early studies of electrode-supported redox polymers employed the cation-exchange material Nafion as a host matrix owing to its convenience and ability to strongly extract and electrostatically bind a wide range of redox-active cations.[1,45−47] Building on this foundation, the cell in Figure 1 was initially tested on Nafion films containing exchanged $MV^{2+}$ ions. $MV^{2+}$ and its reduced radical cation ($MV^{+\bullet}$) have rich vibrational spectra, and when excited near 660 nm, electrogenerated $MV^{+\bullet}$ can be sensitively detected by resonance Raman scattering.[48]

Figure 2 shows Raman spectra that capture the formation of MV radical cation ($MV^{+\bullet}$) as it is electrogenerated from $MV^{2+}$ ions within a Nafion layer supported on a carbon disk electrode. Just before spectral acquisition, the confocal probe volume was translated into the polymer film and positioned approximately 5 $\mu$m from the carbon surface. The initial spectrum was collected with the cell poised at 0.0 V where $MV^{2+}$ is stable. A weak peak at 1652 $cm^{-1}$ is evident and traceable to mixed-ring stretching and in-plane C−C−H bending vibrations of $MV^{2+}$.[48,49] Several bands in the spectrum, those marked with a star symbol, arise from Nafion[26,50] and the broad features centered near 1300 $cm^{-1}$ (carbon D band) and 1620 $cm^{-1}$ (carbon G band) reflect (resonantly enhanced)[51] scattering from the underlying glassy carbon electrode.[37,52] As the potential is stepped toward more

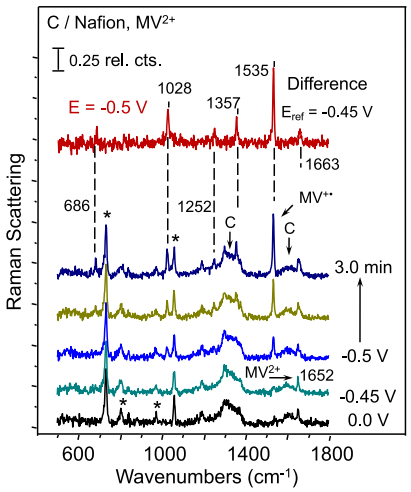


**Figure 2.** In situ Raman spectra recorded from a Nafion film containing exchanged $MV^{2+}$ ions. The film was supported on a carbon disk electrode poised at the indicated potentials ($E$) in 0.1 M KCl. The electrode was held initially at 0.0 V and stepped increasingly negative up to −0.5 V. Peaks marked with an asterisk (*) arise from the Nafion matrix. The dashed vertical lines trace peaks from $MV^{+\bullet}$. The difference spectrum (red, top) shows the uppermost spectrum recorded at −0.5 V (3 min, dark blue) after subtraction of the spectrum recorded at −0.45 V (cyan). See text for further details.

negative values, the spectra remain relatively unchanged (Figure S1) until −0.5 V is reached where a strong feature from electrogenerated $MV^{+\bullet}$ appears at 1535 $cm^{-1}$. When excited near 660 nm, $MV^{+\bullet}$ has notable resonance Raman bands near 1534, 1356, and 1028 $cm^{-1}$.[48] While the first and last of these are prominent in Figure 2, the 1356 $cm^{-1}$ band is not discernible above the carbon background until the potential is held for an extended time period (3 min).

To test the effectiveness of spectral subtraction for removing the carbon interference in these in situ confocal Raman microscopy measurements, the spectrum recorded at −0.45 V was used as the background. The spectrum labeled "difference" in Figure 2 shows the features that remain after applying the subtraction to the uppermost spectrum in the dataset (−0.5 V, 3 min). The carbon interference is eliminated, revealing the 1356 $cm^{-1}$ peak (at 1357 $cm^{-1}$) and several other bands (1663, 1252, and 686 $cm^{-1}$) characteristic of $MV^{+\bullet}$.[48] In studies of surface-derivatized carbon materials, Ray and McCreery used spectral subtraction to reduce the impact of bulk carbon scattering in Raman spectra of covalently bonded probe molecules.[37] The results in Figure 2 show that the approach eliminates the much weaker carbon background interference from the spectra of molecules within the confocal probe volume region[33] when the probe volume location is a few micrometers away from the carbon surface.

The band at 1028 $cm^{-1}$ in Figure 2 brings to light the potential for $MV^{+\bullet}$ dimer formation.[23,48] However, when excited at 660 nm, $MV^{+\bullet}$ generates a strong scattering signal at 1028 $cm^{-1}$ unrelated to the dimer.[48] Instead, a band near 664 $cm^{-1}$ can serve as a marker for the $MV^{+\bullet}$ dimer[48] and its absence in Figure 2 suggests that dimer formation may not be significant under the conditions of the reported experiments.

A cyclic voltammogram recorded with the cell secured to the microscope stage and the electrode positioned for spectral measurements is included in Figure S2. The response is consistent with voltammograms for $MV^{2+}$-modified Nafion


https://doi.org/10.1021/acsmeasuresciau.2c00064
ACS Meas. Sci. Au 2023, 3, 127−133

films on carbon[53] and other all-organic[4] redox polymers. The potential at the midway point between the voltammetric peaks, −0.62 V, matches the formal potential for the $MV^{2+}/MV^{+\bullet}$ couple (−0.62 V on the KCl-saturated Ag/AgCl reference scale).[53] Furthermore, the imbalance in the cathodic and anodic peak currents, the former being somewhat greater than the latter, is in accord with the markedly slower diffusion coefficient of $MV^{+\bullet}$ relative to $MV^{2+}$ in Nafion.[53] The separation between cathodic and anodic peaks is somewhat greater than anticipated compared to the benchmark,[53] reflecting at least in part the differences in material processing. The voltammetry in Figure S2 demonstrates a significant advantage of having an electrochemical cell for in situ Raman measurements that enables conventional electrodes to be used, eliminating the resistive effects that can limit electrochemical measurements with optically transparent electrodes.[26]

The ability to track the reversibility of the $MV^{2+}/MV^{+\bullet}$ couple within the polymer is depicted in Figure S3. Temporally resolved spectra collected at intervals following a potential step show progressive changes in the amount of $MV^{+\bullet}$ present. After stepping from −0.3 to −0.5 V, peaks for $MV^{+\bullet}$ become evident within 20 s and grow as anticipated in response to the advancing diffusion layer within the electrode-supported film.[26] The trend reverses when the potential is stepped to more positive values, 0.0 V in this case, where $MV^{+\bullet}$ oxidation occurs at a diffusion-limited rate. The repeatable behavior depicted in Figure S3 was observed over several oxidation/reduction cycles.

Spectra recorded from an electrode-supported film that displays dimensional change during redox transformations are shown in Figures 3 and 4. Figure 3 tracks the formation of

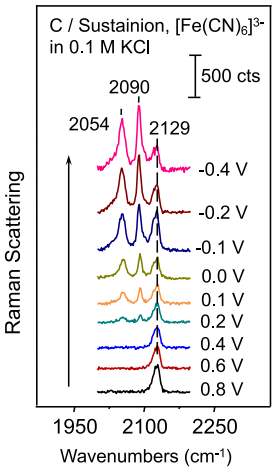


**Figure 3.** In situ Raman spectra recorded from a Sustainion[54] film containing exchanged $Fe(CN)_6^{3-}$ ions. The film was supported on a carbon disk electrode poised at the indicated potentials in 0.1 M KCl. The electrode was held initially at +0.8 V and stepped increasingly negative.

$Fe(CN)_6^{4-}$ from $Fe(CN)_6^{3-}$ ions immobilized within a thin layer of the anion-exchange ionomer Sustainion[54] supported on a carbon disk electrode. The electrode was held initially at 0.8 V and stepped increasingly negative. The region of the ligand C≡N stretching vibrations is plotted in Figure 3. The 2129 $cm^{-1}$ peak contains contributions from the overlapping $\nu_1$ ($A_{1g}$ symmetry) and $\nu_3$ ($E_{2g}$ symmetry) vibrational modes of $Fe(CN)_6^{3-}$, while the peaks at 2090 and 2054 $cm^{-1}$ map to the respective $\nu_1$ and $\nu_3$ stretching vibrations of $Fe(CN)_6^{4-}$ ions.[55,56] Comparing the relative amplitudes of the bands for the two species in Figure 3, the formal potential is expected in the range where the peaks have roughly equal intensity.[26] On this basis, the spectra suggest that the formal potential lies between 0.1 and 0.0 V, negative of the anticipated value (in the 0.25−0.22 V range)[26,57] but consistent with the 100−200 mV negative shift reported for $Fe(CN)_6^{3-}/Fe(CN)_6^{4-}$ ions at electrodes modified by thin films of anion-exchange materials in contact with 0.1 M supporting electrolytes.[57−59] The shift has been attributed to factors that lead to greater stabilization of $Fe(CN)_6^{3-}$ compared to $Fe(CN)_6^{4-}$ ions within the films.[57−59]

Figure 4 displays potential difference spectra that reveal polymer framework structural changes occurring as the film

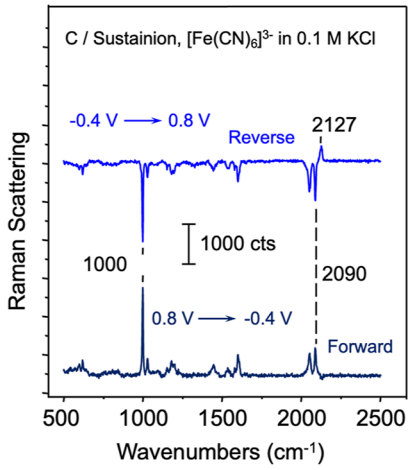


**Figure 4.** Difference spectra showing changes that occur within a Sustainion[54] film containing exchanged $Fe(CN)_6^{3-}$ ions when the potential is first changed from +0.8 to −0.4 V (bottom) and subsequently returned to +0.8 V (top). The film was supported on a carbon disk electrode in 0.1 M KCl.

oxidation state is varied. In progressing from 0.8 to −0.4 V (Figure 4, bottom), the upward bands reflect species whose composition within the confocal probe volume becomes greater at −0.4 V. The pair of peaks near 2090 $cm^{-1}$ trace the formation of $Fe(CN)_6^{4-}$ ions, while the strong peak near 1000 $cm^{-1}$ and several weaker upward peaks toward higher frequency arise from the Sustainion matrix (Figure S4). The appearance of Sustainion bands in the difference spectrum can be attributed to the contraction of the polymer framework as chloride ions transfer from the film into the contacting electrolyte solution in response to the reduction of $Fe(CN)_6^{3-}$ ions.[13,58] In the study of electrode-supported films prepared by entrapment of redox-active transition-metal compounds within inert ionomers,[46,47] it has been shown that small mobile ions derived from the electrolyte redistribute between the film and bulk solution to compensate for the charge imbalance that accompanies changes in the film oxidation state.[13,58] For Sustainion containing electrostatically bound $Fe(CN)_6^{3-}$ ions, the reaction can be depicted as follows

$$(Im^+)_n(Fe(CN)_6^{3-}) + (Im^+)Cl^- + e^- \rightarrow (Im^+)_{(n+1)}(Fe(CN)_6^{4-}) + Cl^-_{(aq)} \quad (1)$$

In eq 1, $(Im^+)$ represents imidazolium sites[54] within the Sustianion matrix that complex $Fe(CN)_6^{3-}$, $Fe(CN)_6^{4-}$, and


https://doi.org/10.1021/acsmeasuresciau.2c00064
ACS Meas. Sci. Au 2023, 3, 127−133

chloride ions, as indicated, and $Cl^-_{(aq)}$ represents the chloride released from the polymer into the electrolyte solution.

The Sustainion matrix peaks in Figure 4 track the movement of chloride ions anticipated from eq 1. The film appears to deswell as chloride is discharged upon reduction of $Fe(CN)_6^{3-}$ at −0.4 V, producing the upward pointing peaks in the lower spectrum of Figure 4. When the direction of the potential excursion is reversed (Figure 4, top), the conversion of $Fe(CN)_6^{4-}$ back to $Fe(CN)_6^{3-}$ draws chloride into the film. The swelling that ensues with the re-entry of chloride ions decreases the concentration of the ionomer within the confocal probe volume, giving downward pointing peaks for the ionomer in the difference spectrum.

In Figure 4 (top), the upward peak at 2127 $cm^{-1}$ and pair of downward peaks near 2090 $cm^{-1}$ signal the formation of $Fe(CN)_6^{3-}$ from $Fe(CN)_6^{4-}$ at 0.8 V. In the bottom spectrum, which tracks the opposite transformation, the 2127 $cm^{-1}$ feature that accompanies $Fe(CN)_6^{3-}$ reduction is weaker than expected. The response may reflect the offsetting effect of increasing $(Im^+)_n(Fe(CN)_6^{3+})$ site concentration within the confocal probe volume as the polymer framework contracts with the progression of the reaction in eq 1.

The difference spectra[33] in Figures 2 and 4 demonstrate the ability to uncover signals of interest that are linked to changes in electrode potential but without subtraction are obscured by strong scattering from the film matrix or underlying electrode. In studies of the $MV^{2+}/MV^{+\bullet}$ redox couple in Nafion, spectral subtraction made it possible to detect clear signatures of $MV^{+\bullet}$ while probing close enough to the electrode to detect background scattering from the underlying carbon. Although not an interferent in studies of the $Fe(CN)_6^{3-}/Fe(CN)_6^{4-}$ couple in Sustainion, spectral subtraction also achieved the removal of broad bands near 1323 and 1600 $cm^{-1}$ (Figure S5) due to bulk carbon. Finally, unlike the sensitivity of the Sustainion matrix (Figure 4), difference spectra calculated over the range of potentials studied in Figure 2 did not contain evidence for Nafion film dimensional change as the potential was varied. Since several factors (i.e., ionomer ion-exchange capacity and redox probe size, charge, and loading) can affect film swelling behavior, further investigation is needed to better understand the different matrix responses of the two redox polymer systems.

## CONCLUSIONS

A precision-machined, microscope-mountable cell that adapts widely available disk electrodes, including low-cost carbon disk electrodes, has enabled in situ confocal Raman microscopy measurements that probe within micrometer-scale thickness electrode-supported redox polymer films. Owing to the high collection efficiency and wavelength reproducibility of the Raman system utilized,[26,29,33] spectral subtraction provided excellent rejection of background interferences and revealed sensitivity toward potential-induced changes in the composition and swelling/deswelling behavior of electrode-supported redox polymers. The advances open opportunities for in situ characterization of strategically designed, leading-edge redox polymers that are pushing the frontiers of energy and chemical synthesis and sensing technologies.[3−6,8,9,12,60] With careful consideration of limiting optical phenomena,[27−30] quantitative, spatially resolved measurements within these materials are possible.

## ASSOCIATED CONTENT

### Supporting Information

The Supporting Information is available free of charge at https://pubs.acs.org/doi/10.1021/acsmeasuresciau.2c00064.

Raman microscopy experimental details; full in situ spectral data sets for MV in Nafion and $Fe(CN)_6^{3-}$ ions in Sustainion, including time-resolved in situ Raman spectra of MV in Nafion; cyclic voltammetry for MV in Nafion; and Raman spectrum of Sustainion (PDF)

## AUTHOR INFORMATION


### Corresponding Author

**Carol Korzeniewski** − *Department of Chemistry and Biochemistry, Texas Tech University, Lubbock, Texas 79409-1061, United States;* orcid.org/0000-0003-3672-0731; Email: carol.korzeniewski@ttu.edu

### Authors

**Jiahe Xu** − *Department of Chemistry and Biochemistry, Texas Tech University, Lubbock, Texas 79409-1061, United States*

**Miharu Koh** − *Department of Chemistry, University of Utah, Salt City, Utah 84112, United States*

**Shelley D. Minteer** − *Department of Chemistry, University of Utah, Salt City, Utah 84112, United States;* orcid.org/0000-0002-5788-2249

Complete contact information is available at: https://pubs.acs.org/10.1021/acsmeasuresciau.2c00064


### Author Contributions

CRediT: **Jiahe Xu** data curation (equal), formal analysis (equal), investigation (equal), methodology (equal), writing-review & editing; **Miharu Koh** data curation (supporting), formal analysis (supporting); **Shelley D. Minteer** conceptualization (equal), funding acquisition (equal), investigation (equal), supervision, writing-review & editing (equal); **Carol Korzeniewski** conceptualization (equal), formal analysis (equal), funding acquisition (equal), investigation (equal), supervision (equal), writing-original draft (equal), writing-review & editing (equal).

### Notes

The authors declare no competing financial interest.

## ACKNOWLEDGMENTS

We gratefully acknowledge financial support from the U.S. National Science Foundation (NSF) through grants CBET-1922956 (C.K.) and CBET-1921075 (S.D.M.) and thank machinists Scott Hiemstra (TTU), Chuck Pfeiffer (TTU), and Tom Gudmundson (UU) for assistance with cell design and fabrication.

## REFERENCES

(1) Murray, R. W.Chemically Modified Electrodes. In *Electroanalytical Chemistry*; Bard, A. J., Ed.; Dekker: New York, 1984; Vol. *13*, pp 191−368.

(2) Murray, R. W. Polymer modification of electrodes. *Annu. Rev. Mater. Sci.* **1984**, *14*, 145−169.

(3) Plumeré, N.; Rüdiger, O.; Oughli, A. A.; Williams, R.; Vivekananthan, J.; Pöller, S.; Schuhmann, W.; Lubitz, W. A redox hydrogel protects hydrogenase from high-potential deactivation and oxygen damage. *Nat. Chem.* **2014**, *6*, 822−827.

(4) Lee, Y. S.; Ruff, A.; Cai, R.; Lim, K.; Schuhmann, W.; Minteer, S. D. Electroenzymatic nitrogen fixation using a MoFe protein system immobilized in an organic redox polymer. *Angew. Chem., Int. Ed.* **2020**, *59*, 16511−16516.
(5) Gossage, Z. T.; Schorr, N. B.; Hernández-Burgos, K.; Hui, J.; Simpson, B. H.; Montoto, E. C.; Rodríguez-López, J. Interrogating Charge Storage on Redox Active Colloids via Combined Raman Spectroscopy and Scanning Electrochemical Microscopy. *Langmuir* **2017**, *33*, 9455−9463.
(6) Mulzer, C. R.; Shen, L.; Bisbey, R. P.; McKone, J. R.; Zhang, N.; Abruña, H. D.; Dichtel, W. R. Superior charge storage and power density of a conducting polymer-modified covalent organic framework. *ACS Cent. Sci.* **2016**, *2*, 667−673.
(7) Fadeev, M.; Ouyang, Y.; Davidson-Rozenfeld, G.; Willner, I. Controlling electrocatalytic, photoelectrocatalytic, and load release processes using soft material-modified electrodes. *J. Electroanal. Chem.* **2022**, *904*, 115926.
(8) Wang, C.; O'Hagan, M. P.; Willner, B.; Willner, I. Bioinspired artificial photosynthetic systems. *Chem. - Eur. J.* **2022**, *28*, No. e202103595.
(9) Sempionatto, J. R.; Jeerapan, I.; Krishnan, S.; Wang, J. Wearable chemical sensors: Emerging systems for on-body analytical chemistry. *Anal. Chem.* **2020**, *92*, 378−396.
(10) Aoki, A.; Heller, A. Electron diffusion coefficients in hydrogels formed of cross-linked redox polymers. *J. Phys. Chem.* **1993**, *97*, 11014−11019.
(11) Glidle, A.; Hillman, A. R.; Ryder, K. S.; Smith, E. L.; Cooper, J.; Gadegaard, N.; Webster, J. R. P.; Dalgliesh, R.; Cubitt, R. Use of neutron reflectivity to measure the dynamics of solvation and structural changes in polyvinylferrocene films during electrochemically controlled redox cycling. *Langmuir* **2009**, *25*, 4093−4103.
(12) Merchant, S. A.; Meredith, M. T.; Tran, T. O.; Brunski, D. B.; Johnson, M. B.; Glatzhofer, D. T.; Schmidtke, D. W. Effect of mediator spacing on electrochemical and enzymatic response of ferrocene redox polymers. *J. Phys. Chem. C* **2010**, *114*, 11627−11634.
(13) Naegeli, R.; Redepenning, J.; Anson, F. C. Influence of supporting electrolyte concentration and composition on formal potentials and entropies of redox couples incorporated in Nafion coatings on electrodes. *J. Phys. Chem.* **1986**, *90*, 6227−6232.
(14) Buttry, D. A.; Ward, M. D. Measurement of interfacial processes at electrode surfaces with the electrochemical quartz crystal microbalance. *Chem. Rev.* **1992**, *92*, 1355−1379.
(15) Porter, M. D. IR external reflection spectroscopy:A probe for chemically modified surfaces. *Anal. Chem.* **1988**, *60*, 1143A−1155A.
(16) Popenoe, D. D.; Stole, S. M.; Porter, M. D. Optical considerations for infrared reflection spectroscopic analysis in the carbon-hydrogen stretching region of monolayer films at an aqueous/metal interface. *Appl. Spectrosc.* **1992**, *46*, 79−87.
(17) Chang, S. C.; Weaver, M. J. In situ infrared spectroscopy at single-crystal metal electrodes:An emerging link between electrochemical and ultrahigh-vacuum surface science. *J. Phys. Chem.* **1991**, *95*, 5391−5400.
(18) Korzeniewski, C.Recent Advances in In Situ Infrared Spectroscopy and Applications in Single Crystal Electrochemistry and Electrocatalysis. In *Diffraction and Spectroscopic Methods in Electrochemistry*; Alkire, R., Kolb, D. M., Lipkowski, J., Ross, P. N., Eds.; Wiley-VCH: Weinheim, 2006; Vol. *9*, pp 233−268.
(19) Su, Z. F.; Ran, X. Q.; Leitch, J. J.; Schwan, A. L.; Faragher, R.; Lipkowski, J. How valinomycin ionophores enter and transport $K^+$ across model lipid bilayer membranes. *Langmuir* **2019**, *35*, 16935−16943.
(20) Zhang, Y.-J.; Su, Z.-F.; Li, J.-F.; Lipkowski, J. What vibrational spectroscoy tells about water structure at the electrified palladium-water interface. *J. Phys. Chem. C* **2020**, *124*, 13240−13248.
(21) Blackburn, T. J.; Tyler, S. M.; Pemberton, J. E. Optical spectroscopy of surfaces, interfaces, and thin films. *Anal. Chem.* **2022**, *94*, 515−558.
(22) Kruse, F.; Nguyen, A. D.; Dragelj, J.; Heberle, J.; Hildebrandt, P.; Mroginski, M. A.; Weidinger, I. M. A resonance Raman marker band characterizes the slow and fast form of cytochrome *c* oxidase. *J. Am. Chem. Soc.* **2021**, *143*, 2769−2776.
(23) Wang, B.; daFonseca, B. G.; Brolo, A. G.; Sagara, T. In situ surface-enhanced Raman scattering spectroscopic study of a redox-active deformable hydrogel on a roughened Au electrode surface. *Chem. Lett.* **2021**, *50*, 467−470.
(24) Kollath, V. O.; Liang, Y.; Mayer, F. D.; Ma, X.; Korzeniewski, C.; Karan, K. Model-based analyses of confined polymer electrolyte nanothin films experimentally probed by polarized ATR−FTIR spectroscopy. *J. Phys. Chem. C* **2018**, *122*, 9578−9585.
(25) Stiles, P. L.; Dieringer, J. A.; Shah, N. C.; Van Duyne, R. P. Surface-enhanced Raman spectroscopy. *Annu. Rev. Anal. Chem.* **2008**, *1*, 601−626.
(26) Korzeniewski, C.; Peterson, E. M.; Kitt, J. P.; Minteer, S. D.; Harris, J. M. Adapting confocal Raman microscopy for in situ studies of redox transformations at electrode-electrolyte interfaces. *J. Electroanal. Chem.* **2021**, *896*, 115207.
(27) Everall, N. J. Confocal Raman microscopy: Common errors and artefacts. *Analyst* **2010**, *135*, 2512−2522.
(28) Bridges, T.; Houlne, M.; Harris, J. M. Spatially resolved analysis of small particles by confocal Raman microscopy: Depth profiling and optical trapping. *Anal. Chem.* **2004**, *76*, 576−584.
(29) Korzeniewski, C.; Kitt, J. P.; Bukola, S.; Creager, S. E.; Minteer, S. D.; Harris, J. M. Single layer graphene for estimation of axial spatial resolution in confocal Raman microscopy depth profiling. *Anal. Chem.* **2019**, *91*, 1049−1055.
(30) Deabate, S.; Huguet, P.; Morin, A.; Gebel, G.; Lanteri, Y.; Peng, Z.; Sutor, A. K. Raman microspectroscopy as a useful tool for in situ and operando studies of water transport in perfluorosulfonic membranes for PEMFCs. *Fuel Cells* **2014**, *14*, 677−693.
(31) Kitt, J. P.; Harris, J. M. Confocal Raman microscopy for in situ measurement of octanol-water partitioning within pores of individual $C_{18}$-functionalized chromatographic particles. *Anal. Chem.* **2015**, *87*, 5340−5347.
(32) Bryce, D. A.; Kitt, J. P.; Harris, J. M. Confocal Raman microscopy for label-free detection of protein-ligand binding at nanopore-supported phospholipid bilayers. *Anal. Chem.* **2018**, *90*, 11509−11516.
(33) Myres, G. J.; Peterson, E. M.; Harris, J. M. Confocal Raman microscopy enables label-free, quantitative, and structurally informative detection of DNA hybridization at porous silica surfaces. *Anal. Chem.* **2021**, *93*, 7978−7986.
(34) Myres, G. J.; Kitt, J. P.; Harris, J. M. Inter-leaflet phospholipid exchange impacts the ligand density available for protein binding at supported lipid bilayers. *Langmuir* **2022**, *38*, 6967−6976.
(35) Steimecke, M.; Seiffarth, G.; Bron, M. In situ characterization of Ni and Ni/Fe thin film electrodes for oxygen evolution in alkaline media by a Raman-coupled scanning electrochemical microscope setup. *Anal. Chem.* **2017**, *89*, 10679−10686.
(36) Zeng, Z.-C.; Hu, S.; Huang, S.-C.; Zhang, Y.-J.; Zhao, W.-X.; Li, J.-F.; Jiang, C.; Ren, B. Novel electrochemical Raman spectroscopy enabled by water immersion objective. *Anal. Chem.* **2016**, *88*, 9381−9385.
(37) Ray, K. G., III; McCreery, R. L. Characterization of the surface carbonyl and hydroxyl coverage on glassy carbon electrodes using Raman spectroscopy. *J. Electroanal. Chem.* **1999**, *469*, 150−158.
(38) Duan, J.; Goswami, G.; Patwardhan, S.; Hupp, J. T. Does the mode of metal-organic framework/electrode adhesion determine rates for redox-hopping-based charge transport within thin-film metal-organic frameworks? *J. Phys. Chem. C* **2022**, *126*, 4601−4611.
(39) Williams, K. P. J.; Pitt, G. D.; Batchelder, D. N.; Kip, B. J. Confocal Raman microspectroscopy using a stigmatic spectrograph and CCD detector. *Appl. Spectrosc.* **1994**, *48*, 232−235.
(40) Wang, Y.; McCreery, R. L. Evaluation of a diode laser/charge coupled device spectrometer for near-infrared Raman spectroscopy. *Anal. Chem.* **1989**, *61*, 2647−2651.
(41) Fryling, M. A.; Frank, C. J.; McCreery, R. L. Intensity calibration and sensitivity comparisons for CCD/Raman spectrometers. *Appl. Spectrosc.* **1993**, *47*, 1965−1974.


https://doi.org/10.1021/acsmeasuresciau.2c00064
*ACS Meas. Sci. Au* 2023, 3, 127−133

(42) Choquette, S. J.; Etz, E. S.; Hurst, W. S.; Blackburn, D. H.; Leigh, S. D. Relative intensity correction of Raman spectrometers: NIST SRMs 2241 through 2243 for 785 nm, 532 nm, and 488 nm/514.5 nm excitation. *Appl. Spectrosc.* **2007**, *61*, 117−129.
(43) Brandt, N. N.; Brovko, O. O.; Chikishev, A. Y.; Paraschuk, O. D. Optimization of the rolling-circle filter for Raman background subtraction. *Appl. Spectrosc.* **2006**, *60*, 288−293.
(44) Seki, H.; Kunimatsu, K.; Golden, W. G. A thin-layer electrochemical cell for infrared spectroscopic measurements of the electrode/electrolyte interface. *Appl. Spectrosc.* **1985**, *39*, 437−443.
(45) White, H. S.; Leddy, J.; Bard, A. J. Polymer films on electrodes. 8. Investigation of charge-transport mechanisms in Nafion polymer modified electrodes. *J. Am. Chem. Soc.* **1982**, *104*, 4811−4817.
(46) Gellett, W. L.; Knoche, K. L.; Rathuwadu, N. P. W.; Leddy, J. Electron hopping of tris (2,2'-bipyridyl) transition metal complexes $M(bpy)_3^{2/3}$ in Nafion. *J. Electrochem. Soc.* **2016**, *163*, H588−H597.
(47) Oberbroeckling, K. J.; Dunwoody, D. C.; Minteer, S. D.; Leddy, J. Density of Nafion exchanged with transition metal complexes and tetramethyl ammonium, ferrous, and hydrogen ions: Commercial and recast films. *Anal. Chem.* **2002**, *74*, 4794−4799.
(48) Forster, M.; Girling, R. B.; Hester, R. E. Infrared, Raman and resonance Raman investigations of methylviologen and its radical cation. *J. Raman Spectrosc.* **1982**, *12*, 36−48.
(49) Romanova, J.; Liégeois, V.; Champagne, B. Analysis of the resonant Raman spectra of viologens and of their radical cations using range-separated hybrid density functionals. *J. Phys. Chem. C* **2014**, *118*, 12469−12484.
(50) Gruger, A.; Régis, A.; Schmatko, T.; Colomban, P. Nanostructure of Nafion membranes at different states of hydration−An IR and Raman study. *Vib. Spectrosc.* **2001**, *26*, 215−225.
(51) Ferrari, A. C.; Basko, D. M. Raman spectroscopy as a versatile tool for studying the properties of graphene. *Nat. Nanotechnol.* **2013**, *8*, 235−246.
(52) Wang, Y.; Alsmeyer, D. C.; McCreery, R. L. Raman spectroscopy of carbon materials:Structural basis of observed spectra. *Chem. Mater.* **1990**, *2*, 557−563.
(53) Chen, L.; Lin, C.; Compton, R. G. Electrochemical characterisation and comparison of transport in Nafion films and particles. *Phys. Chem. Chem. Phys.* **2019**, *21*, 607−616.
(54) Kutz, R. B.; Chen, Q.; Yang, H.; Sajjad, S. D.; Liu, Z.; Masel, I. R. Sustainion imidazolium-functionalized polymers for carbon dioxide electrolysis. *Energy Technol.* **2017**, *5*, 929−936.
(55) Nakagawa, I.; Shimanouchi, T. Infrared spectroscopic study on the co-ordination bond - II Infrared spectra of octahedral metal cyanide complexes. *Spectrochim. Acta* **1962**, *18*, 101−113.
(56) Nakamoto, K.*Infrared and Raman Spectra of Inorganic and Coordination Compounds*, 6th ed.; Wiley: New York, 2009.
(57) Shi, Y.; Slaterbeck, A. F.; Seliskar, C. J.; Heineman, W. R. Spectroelectrochemical sensing based on multimode selectivity simultaneously achievable in a single device. 1. Demonstration of concept with ferricyanide. *Anal. Chem.* **1997**, *69*, 3679−3686.
(58) Redepenning, J.; Anson, F. C. Permselectivities of polyelectrolyte electrode coatings as inferred from measurements with incorporated redox probes of concentration cells. *J. Phys. Chem.* **1987**, *91*, 4549−4553.
(59) Zhuang, X.; Wang, D.; Lin, Y.; Yang, L.; Yu, P.; Jiang, W.; Mao, L. Strong interaction between imidazolium-based polycationic polymer and ferricyanide: Toward redox potential regulation for selective in vivo electrochemical measurements. *Anal. Chem.* **2012**, *84*, 1900−1906.
(60) Malapit, C. A.; Prater, M. B.; Cabrera-Pardo, J. R.; Li, M.; Pham, T. D.; McFadden, T. P.; Blank, S.; Minteer, S. D. Advances on the merger of electrochemistry and transition metal catalysis for organic synthesis. *Chem. Rev.* **2022**, *122*, 3180−3218.


https://doi.org/10.1021/acsmeasuresciau.2c00064
*ACS Meas. Sci. Au* 2023, 3, 127−133